Nanoimprinted semiconducting polymer films with 50 nm features and their application to organic heterojunction solar cells

2008 Nanotechnology 19 424016

(http://iopscience.iop.org/0957-4484/19/42/424016)

Nanotechnology **19** (2008) 424016 (6pp) doi:10.1088/0957-4484/19/42/424016

Nanoimprinted semiconducting polymer films with 50 nm features and their application to organic heterojunction solar cells

D Cheyns[1,2], K Vasseur[1,3], C Rolin[1], J Genoe[1], J Poortmans[1,2] and P Heremans[1,2]

[1] IMEC vzw, Kapeldreef 75, 3001 Leuven, Belgium
[2] ESAT, Katholieke Universiteit Leuven, Kasteelpark Arenberg 10, B-3001 Leuven, Belgium
[3] MTM, Katholieke Universiteit Leuven, Kasteelpark Arenberg 44, B-3001 Leuven, Belgium

E-mail: david.cheyns@imec.be

Received 11 July 2008, in final form 11 August 2008
Published 25 September 2008
Online at stacks.iop.org/Nano/19/424016

Abstract

Nanoimprint lithography is used to directly pattern the conjugated polymer semiconductor poly(3-hexylthiophene) (P3HT). We obtain trenches with aspect ratios up to 2 and feature sizes as small as 50 nm in this polymer. The application to organic solar cells is shown by creating an interpenetrated donor–acceptor interface, based on P3HT and N, N'-ditridecyl-3,4,9,10-perylenetetracarboxylic diimide (PTCDI-C_{13}), deposited from the vapor phase to reduce shadow effects. A planarizing layer of spin-coated zinc oxide (ZnO) nanoparticles is used to reduce the roughness of the layer stack. The response of the photovoltaic devices follows the increased interface area, up to a 2.5-fold enhancement.

1. Introduction

An important breakthrough for organic solar cells was the first bilayer device [1] in 1986. Earlier organic photovoltaic devices relied upon a single layer of conjugated semiconductor, in which high electrical fields are needed to dissociate excitons. In contrast, the use of a heterojunction of two materials with different energy levels can induce efficient exciton dissociation at the interface between them. The light-generated excitons need to diffuse to the donor–acceptor interface to reach the dissociation center. The exciton diffusion length (L_D) limits the width of the effective photo-active region (see figure 1(a)). Nevertheless, by clever layer optimization to increase the optical field inside the device, relatively efficient devices have been demonstrated [2–4]. The second breakthrough was the introduction of the bulk heterojunction concept [5, 6]. The photo-active layer consists of a mixture of donor and acceptor materials, as such creating dissociation centers everywhere within the active layer (figure 1(b)). Exciton diffusion will not limit the device performance, but carrier extraction is an issue. Inside the layer, two major problems arise: (1) shunt paths of a single material (being donor or acceptor) connecting both contacts, and (2) isolated islands of material. The shunt paths will reduce the parallel resistance and this has a direct effect on the cell's performance [7–9]. The isolated islands can trap carriers, which will not contribute to the photo response. The choice of solvent and post-annealing steps influence the carrier collection efficiency, but the exact effect is difficult to predict beforehand [10, 11].

Here, we present a hybrid between a planar and bulk heterojunction solar cell, where a controlled morphology combines the advantages of both. A separate deposition of donor and acceptor material makes it possible to optimize each, and to reduce shunts or isolated islands, while the interpenetrating network provides dissociation centers throughout the whole layer (figure 1(c)). Ideally, the width of the trench should be in the range of the exciton diffusion length [12], or $w_a \approx L_{D,A}$ and $w_D \approx L_{D,D}$. In this case, every created exciton is within an exciton diffusion length of a dissociation center. The depth of the trenches, d_i, should be as large as possible, with the absorption length of the organic semiconductor as a good guideline. Examples in the literature use vapor phase deposition [13] or nanoimprint lithography [14] to make the interpenetrating network.

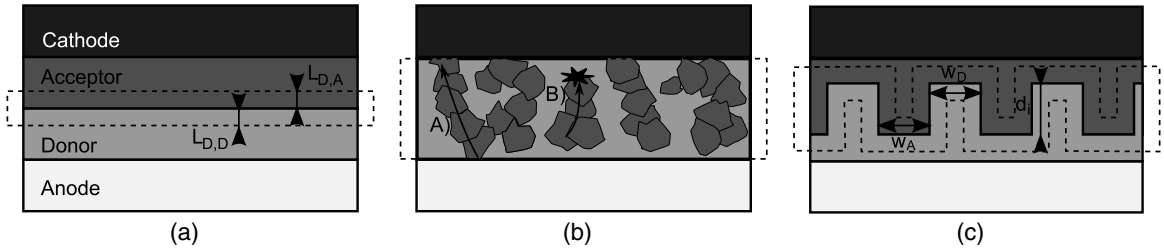

Figure 1. Different architectures of organic solar cells: (a) a planar heterojunction solar cell, (b) a bulk heterojunction and (c) a solar cell with an interpenetrating network. The dashed areas are the photo-active areas, determined by the exciton diffusion lengths of the donor material ($L_{D,D}$) and acceptor material ($L_{D,A}$). Two possible losses of performance are shown for (b): (A) are shunting paths and (B) are isolated islands. The important dimensions in (c) are the depth of the trench (d_i) and the width of the trench in the donor (w_D) and acceptor (w_A).

In this paper we use nanoimprinting to mold the well established donor material poly(3-hexylthiophene) (P3HT).

Nanoimprint lithography uses a mold with fine structures to transfer these nanostructures by imprinting them into a polymer [15, 16]. Although the fabrication of a mold with fine structures is time-consuming and expensive (mostly done via e-beam lithography), every mold can be used many times to reproduce the nanostructures, even allowing the mold to be cloned in a fast and inexpensive process [17]. Nanoimprint lithography is not restricted to small areas, and roll-to-roll processing [18, 19] and large area imprinting [20, 17] are possible. Structures below 10 nm are demonstrated in the literature [21, 22], making nanoimprint lithography a candidate to challenge regular photo-lithography. Moreover, these small dimensions are of the order of the exciton diffusion length of organic materials, making it a promising technique for interpenetrated organic solar cells. We present imprinted P3HT layers with feature size down to 50 nm and aspect ratios up to 2. The subsequent step of applying the acceptor was done in the vapor phase rather than from solution, to avoid dissolution of the extremely fine nanoimprinted features of the donor layer. Direct evaporation of the cathode resulted in very poor yield, therefore we introduce a planarization layer on the donor–acceptor structure, consisting of an acetone-soluble metal-oxide nanoparticle ink. We show that the increase in photocurrent is proportional to the increase in the effective area of the folded heterojunction.

2. Experimental details

Glass substrates with patterned indium tin oxide (ITO, Merck Display Technology, $\rho < 20\ \Omega/\square$) were cleaned with soap, deionized water, isopropanol and acetone. A 15 min UV–ozone clean directly prior to spin coating of subsequent layers completed the cleaning procedure. In order to reduce the injection barrier [23], and hence the resistance of the device [24], the substrates were covered with a spin-coated 0.45 μm filtered poly(3,4-ethylenedioxythiophene):poly(styrenesulfonate) (PEDOT:PSS) solution, purchased from H C Starck, at 3000 rpm for 30 s to produce a 30 nm thick layer. The substrates were subsequently heated on a hotplate in air at 120 °C for 10 min to remove excess water. Different mass-to-volume ratios (10–20 mg ml^{-1} solvent) of the donor material P3HT (Rieke) were dissolved in chlorobenzene. The solution was spin-coated inside a nitrogen atmosphere to form layers ranging from 20 to 80 nm thick.

A differential scanning calorimeter (T. A. Instruments 1920) was used to provide information on the glass transition temperature of P3HT. The material was loaded in an aluminum crucible. The heat flux was measured as a function of temperature, which was first increased from 0 to 250 °C at a rate of 10 °C min^{-1} and was lowered after a stabilizing period of 3 min from 250 to 0 °C at the same rate.

The imprint molds used were created by e-beam lithography. The molds, with a layer stack of silicon, silicon oxide and silicon nitride, have a pitch ranging from 200 to 100 nm, with a trench ratio of 50% and a trench depth of 100 nm. The resulting aspect ratios (depth versus width of the trench) are in between 1 and 2. Prior to use, the molds were cleaned with a mixture of hydrogen peroxide and sulfuric acid (H_2O_2:H_2SO_4 3:7) to remove possible contamination. On the clean surface of the mold, a silane (1H,1H,2H,2H-perfluorodecyltrichlorosilane, or FDTS) was deposited from the vapor phase to create an anti-sticking layer [25, 26].

Nanoimprinting was done with a manual two-column hydraulic press, equipped with temperature controllable plates (P/O/Weber), and located in a nitrogen atmosphere. The sample and mold, sandwiched between two thermally conductive soft-silicone pads to enhance the thermal contact and to reduce local stress effects, were placed on a hot chuck, preheated to 120 °C, and a constant pressure of 14 MPa was applied for 15 min. Subsequently, the whole system was cooled down, and the pressure was released when $T < 40$ °C. The mold could easily be removed after use.

The perylene derivative N,N'-ditridecyl-3,4,9,10-perylenetetracarboxylic diimide (PTCDI-C_{13}, Aldrich) was used as an acceptor molecule, deposited by organic vapor phase deposition (OVPD) [13, 27, 28]. The source cell temperature was set to 360 °C and a preheated nitrogen carrier gas flow of 200 sccm (cubic centimeters per minute at STP) was blown through the source cell. The source flow was diluted with a supplemental preheated nitrogen carrier gas flow so that the total flow was 1000 sccm. At the entrance of the deposition chamber, the gas was evenly distributed onto the substrate by use of a showerhead. The deposition rate was 1.3 Å s^{-1} at a growth pressure of 5 Torr.

Zinc oxide (ZnO) nanoparticles dispersed in acetone (10 mg ml^{-1}) were spin-coated (3000 rpm for 60 s) in order

to obtain 40 nm thick layers. The photovoltaic devices were finished with a 100 nm thick ytterbium (Yb) layer, thermally evaporated in an ultra high vacuum (base pressure $<1 \times 10^{-8}$ Torr) as the cathode, to create a device area of 3 mm^2. The transport between the depositions of the different materials was done in nitrogen-filled boxes, but in between different steps the devices saw air for 5–30 s.

Ellipsometric measurements were carried out with a variable angle spectroscopic ellipsometer (GES5, Sopra). Atomic force microscopy (AFM) images were performed on a Picoscan PicoSPM LE scanning probe microscope in tapping mode. A dual beam scanning electron microscope/focused-ion beam (SEM/FIB) (FEI Nova 600 Nanolab) was employed to create a cross-section of the multilayer device. To protect the underlying layers during ion milling, a thin layer of Pt was deposited *in situ*. Subsequently, the cross-section was made by tilting the sample to 52° and the initial trench was cut with the 9300 pA aperture. High resolution SEM images were produced with a Philips XL30 microscope.

Photovoltaic characteristics were measured in a nitrogen atmosphere with an Agilent 4156C parameter analyzer using a LOT-Oriel solar simulator equipped with a 1000 W xenon arc lamp and optical filters to simulate the 100 mW cm^{-2} AM1.5D solar spectrum. The light power was calibrated using a silicon detector and a band pass filter (KG3, LOT-Oriel).

3. Results and discussion

Nanoimprinting can be achieved on a thermoplastic polymer, which is deposited on a hard substrate and heated above its glass transition temperature (T_g). Above this temperature, the polymer chains become more flexible and can flow, at which moment a pre-patterned mold is pressed into the polymer. A high pressure is maintained, deforming the polymer both elastically and inelastically. If the right temperature, pressure and time is chosen, the inelastic deformation is the more important one. The polymer chains creep away from the high pressure areas to the low pressure areas, causing the polymer layer to follow the topography of the mold. In a last step, the system is cooled down below T_g, after which the mold can be removed.

Our goal was to make trenches directly in an optically active material, P3HT, which has been successfully used as active donor material, with absorption between 450 and 650 nm [29]. The glass temperature of a polymer can be measured with differential scanning calorimetry (DSC). This is a thermoanalytical technique in which the heat flux required to increase the temperature of a sample and a reference are measured as a function of temperature. The relative amount of heat required to increase the temperature of the sample indicates certain physical transitions. The result of a DSC experiment (as described above) for regioregular P3HT can be seen in figure 2. A large dip, with an onset around 200 °C and a minimum around 225 °C, corresponds to an endothermic process, which requires more heat to raise the temperature further. This peak indicates the melting point of P3HT, and by integrating the peak the corresponding enthalpy of transition can be calculated. In the literature, similar values are obtained,

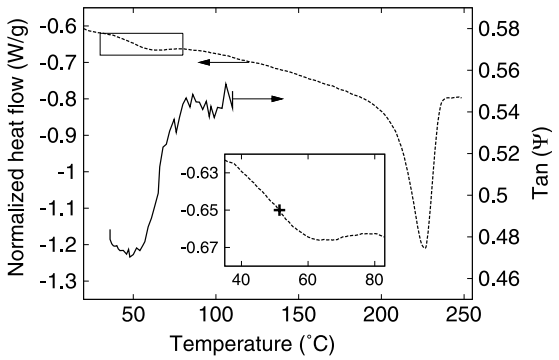

Figure 2. Differential scanning calorimetry measurement on P3HT in powder form (dashed line, left y-axis), and variation of the ellipsometer parameter tan Ψ with temperature, measured on a 50 nm thick P3HT sample on Si/SiO_2 (straight line, right y-axis). During the ellipsometric measurement, the temperature ramp speed was 10 °C min^{-1}; an angle of incidence 75° and a wavelength of 670 nm were used. Inset: zoom of the DSC measurement, with T_g determined by the point of inflection.

while the values can differ depending on heating up or cooling down, and the ramping speed [30–32]. The glass transition can be seen as a step in the DSC plot, as this transition is not a formal phase change but occurs due to a change in heat capacity. The glass transition temperature of P3HT, where the polymer changes from a glassy state to a rubbery state, occurs around a temperature of 51 °C (as determined by the point of inflection of the DSC data; see inset of figure 2). The glass transition temperature is known to depend on the molecular weight of the polymer and on the rate of heating or cooling. Values in the literature range from 12 °C [30] to 110 °C [32]. It should be noted that the different values may correspond to differences in regioregularity and molecular weight of P3HT.

Another way of determining T_g is by the use of ellipsometry [33]. In this case, the incident angle and the wavelength of the light used in the ellipsometric measurement are fixed. The sample is placed on a controllable hot stage. During heating, the change in the two measured parameters (Ψ and Δ) is tracked. The result for a 50 nm thick P3HT sample, ramped at 10 °C min^{-1}, shows a clear change in these parameters (see tan(Ψ) in figure 2) starting from 50 °C, corresponding with the change seen for DSC. We conclude that T_g for the material used is located around 50 °C.

AFM measurements of the imprinted layer confirm good processing, with trenches up to 95 nm deep and a pitch of 140 nm (see figure 3(a)). On a larger scale, small defects are visible, but these are negligible compared to the imprinted area (below 1%). The width of the trenches, as measured by AFM, is 30 nm at the bottom, while the imprinted feature size of the mold is 70 nm. The difference can be attributed to (1) the elastic relaxation after imprinting, and (2) the limitations of the AFM tip. The elastic relaxation can be estimated by the depth of the trenches in the polymer versus the depth of the trenches in the mold. A 5 nm difference is observed, and this could be related to the elastic relaxation after imprinting. However, the error due to convolution of the AFM tip with the topography can be larger than this relaxation. Typical AFM tips have a tip radius of 10 nm, but the aspect ratio is only 5:1. For a steep

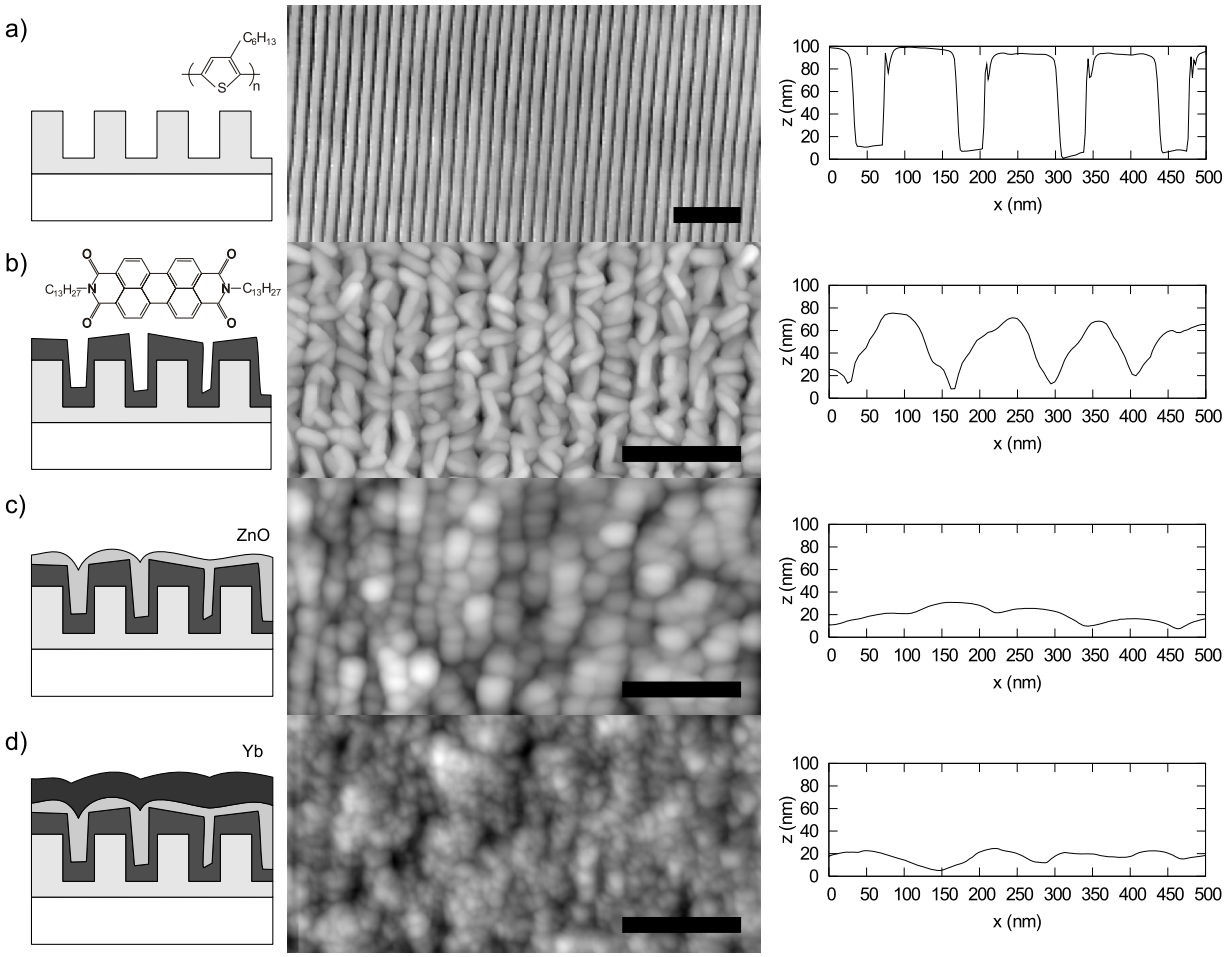

Figure 3. Process flow of the photovoltaic devices presented in this paper. Left: schematic diagram and molecular structure. Middle: AFM measurements with a scale bar equal to 500 nm. Right: cross-sections taken from the AFM measurements. The different steps are: (a) an imprinted 80 nm thick P3HT layer, using a mold with a pitch of 140 nm (70 nm peak, 70 nm valley) and a depth of 100 nm; (b) including a 50 nm thick PTCDI-C_{13} layer, deposited from OVPD; (c) spin-coating a 40 nm thick ZnO layer; and (d) evaporating 100 nm Yb on top of the previous layers.

edge of 100 nm in the measured sample, the induced error can be up to 20 nm. Tips with a high aspect ratio (e.g. using a carbon nanotube at the tip ending [34, 35]) can decrease this error, but these tips tend to stick on the edge of the trenches by van der Waals force, inducing even bigger errors.

The choice of acceptor molecule is limited by the deposition method. The high aspect ratio of the imprinted P3HT trenches makes it difficult to use anisotropic deposition methods like organic molecular beam deposition (OMBD). Shadow effects could reduce the actual donor/acceptor interface. A more isotropic deposition method is the gas transport-based OVPD [13]. As the transport occurs with hot inert nitrogen gas at low pressure, the effective path length of the molecules is much smaller than the case of OMBD. The scattering of the molecules makes it possible to fill up all the gaps. We chose the perylene derivative N,N'-ditridecyl-3,4,9,10-perylenetetracarboxylic diimide (PTCDI-C_{13}; see inset in figure 3(b)) as the acceptor molecule, deposited in a home-built OVPD system [27].

The resulting topography of a 80 nm thick P3HT film, imprinted with a mold of pitch 140 nm and covered with 50 nm PTCDI-C_{13} is shown in figure 3(b). A remarkable feature appears: PTCDI-C_{13} nucleates preferentially on top of the P3HT trenches. Small PTCDI-C_{13} crystals with a length of 100–130 nm and a width of 40–50 nm are formed. Although an isotropic deposition was expected to decrease the initial P3HT roughness, the height profile shows a peak-to-valley of 80 nm, which is only slightly smaller than the peak-to-valley ratio of the imprinted structures (95 nm). Nevertheless, SEM measurements revealed that PTCDI-C_{13} material is effectively deposited at the bottom of the trenches as well (figure not shown).

Cathode deposition on top of this rough interface resulted in metal lines that are not always connected, or which give rise to highly resistive contacts. Reliably contacting the acceptor layer proved to require an electron-conducting planarizing layer on top of the PTCDI-C_{13}. For this function we use the conductive metal-oxide, zinc oxide (ZnO). This material is known for its n-type behavior, and it is transparent. ZnO is already successfully used as acceptor material for bulk heterojunction solar cells in combination with poly[2-methoxy-5-(2′-ethyl-hexyloxy)-*p*-phenylene vinylene] (MEH-PPV) [36],

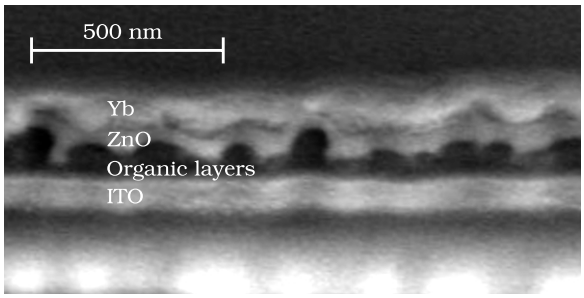

Figure 4. Cross-sectional SEM picture. The vertical cut through all the layers is made by FIB.

Table 1. Structure, relative interface area A/A_0 and extracted characteristics for different P3HT/PTCDI-C_{13} devices.

Structure	A/A_0	V_{oc} (mV)	I_{sc} (mA cm^{-2})	FF (%)	η (%)
Planar	1	406	0.32	53	0.07
70/70 40 nm	1.5	398	0.45	53	0.096
50/50 40 nm	1.7	390	0.48	55	0.104
50/50 100 nm	3	220	0.74	25	0.04

but not so well with P3HT [37]. ZnO has also been used as an optical spacer, both for single cells [38] and as an interconnecting layer in tandem cells [39]. ZnO nanoparticles are dispersed in acetone, a solvent that does not dissolve the underlying organic layers.

AFM pictures of ZnO nanoparticles spin-coated on top of a nanoimprinted P3HT layer and PTCDI-C_{13} deposition (figure 3(c)) show a much smoother surface topography. The imprinted structures almost disappear, and the subsequent Yb deposition creates a smooth metal layer (see figure 3(d)). A cross-sectional SEM picture is seen in figure 4. The difference between the different organic materials cannot be seen. The ZnO nanoparticles fill up the gaps where the total organic layer is very thin, and protect the device from shunts during the subsequent metal evaporation. Furthermore, the metal layer made on top of the ZnO is much smoother, and the conductivity is higher (figure not shown).

Complete imprinted solar cells are successfully fabricated by combining all the previous steps. The extracted parameters for devices illuminated with simulated solar light are given in table 1, while the increase in current for the imprinted devices is plotted in figure 5. As a reference, a planar structure with 20 nm P3HT is taken. The relative increase in the donor–acceptor interface area is calculated by assuming a residual layer of 5 nm. In this case, a 20 nm thick P3HT layer, imprinted with a mold of pitch 100 nm, forms trenches with a depth of 30 nm. This leads to a relative increase in interface area of 60%. The corresponding increase in current is actually higher (70%), probably due to a changing light field distribution inside the structure [40]. Although imprinted devices with a high aspect ratio suffered from a high series resistance and shunts, leading to low FF and V_{oc}, an increase in I_{sc} is still visible, yielding a 150% increase for a device consisting of a 100 nm thick P3HT layer, imprinted with a 100 nm pitch mold.

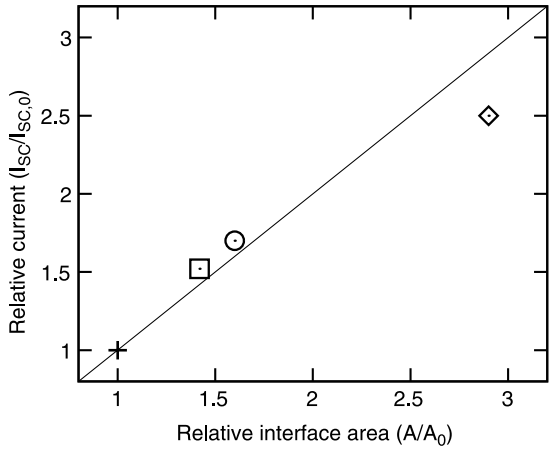

Figure 5. Relative increase in current of nanoimprinted organic solar cells. The reference is a planar device with 20 nm P3HT/50 nm PTCDI-C_{13}/40 nm ZnO/100 nm Yb, with an interface area A_0. The relative interface areas are calculated assuming a residual layer of 5 nm. The imprinted solar cells have the same layer thickness as the planar one, except for the P3HT, with: ⊡, 20 nm P3HT using a 140 nm pitch mold; ⊙, 20 nm P3HT using a 100 nm pitch mold; and ⋄, 55 nm P3HT using a 100 nm pitch mold.

4. Conclusion

Organic solar cells with an interpenetrating donor–acceptor network based on P3HT and PTCDI-C_{13} have been realized. This idealized bulk heterojunction type device is made of nanoimprinted P3HT layers. Substrates covered with P3HT are heated above the glass temperature, which is determined by DSC and ellipsometry to be around 50–60 °C. Features as small as 50 nm could be imprinted to a depth of 100 nm. An elastic relaxation of 5 nm is estimated from AFM measurements, and this will limit the smallest obtainable feature. In a next step, the acceptor material PTCDI-C_{13} is deposited from the gas phase. The molecules are transported by an inert gas, flowing through all the gaps. Remarkably, PTCDI-C_{13} tends to create crystalline structures on the top of the imprinted trenches, although some crystals were visible at the bottom. As a consequence, the topography of the organic layers is extremely rough, making it impossible to create a good metal contact on top of the layers. An intermediate planarizing layer is needed. The chosen material, ZnO nanoparticles dispersed in an acetone solution, is spin-coated on top of the organic layers to fill up the remaining gaps. Metal contacts made on top of this spin-coated layer suffer less from shunt or resistance effects compared to the devices without ZnO. In the end, the light-generated current for imprinted organic solar cells increases with increasing donor–acceptor area. We succeeded in obtaining a 2.5-fold enhancement of short-circuit current in nanoimprinted devices as compared to planar junctions. By using a material set with higher exciton diffusion lengths, further increases in current are expected.

Acknowledgments

This work was supported by the EU Integrated Project NAIMO (no. NMP4-CT-2004-500355). We thank J Gilot for providing

the ZnO ink and J Moonens for fabrication of the nanoimprint molds. Furthermore, we thank M Seo for help with SEM/FIB and D Winant for the DSC measurements.

References

[1] Tang C W 1986 Two-layer organic photovoltaic cell *Appl. Phys. Lett.* **48** 183–5

[2] Peumans P and Forrest S R 2001 Very-high-efficiency double-heterostructure copper phtalocyanine–C_{60} photovoltaic cells *Appl. Phys. Lett.* **79** 126–8

[3] Yoo S, Domercq B and Kippelen B 2004 Efficient thin-film organic solar cells based on pentacene/C_{60} heterojunctions *Appl. Phys. Lett.* **85** 5427–9

[4] Gommans H H P, Cheyns D, Aernouts T, Girotto C, Poortmans J and Heremans P 2007 Electro-optical study of subphthalocyanine in a bilayer organic solar cell *Adv. Funct. Mater.* **17** 2653–8

[5] Hiramoto M, Fujiwara H and Yokoyama M 1991 Three-layered organic solar cell with a photoactive interlayer of codeposited pigments *Appl. Phys. Lett.* **58** 1062–4

[6] Yu G, Gao J, Hummelen J C, Wudl F and Heeger A J 1995 Polymer photovoltaic cells: enhanced efficiencies via a network of internal donor–acceptor heterojunctions *Science* **270** 1789–91

[7] Yoo S, Domercq B and Kippelen B 2005 Intensity-dependent equivalent circuit parameters of organic solar cells based on pentacene and C_{60} *J. Appl. Phys.* **97** 103706

[8] Mazhari B 2006 An improved solar cell circuit model for organic solar cells *Sol. Energy Mater. Sol. Cells* **90** 1021–33

[9] Rand B P, Burk D P and Forrest S R 2007 Offset energies at organic semiconductor heterojunctions and their influence on the open-circuit voltage of thin-film solar cells *Phys. Rev.* B **75** 115327

[10] Shaheen S E, Brabec C J and Sariciftci N S 2001 2.5% efficient organic plastic solar cells *Appl. Phys. Lett.* **78** 841–3

[11] Kim Y, Choulis S A, Nelson J, Bradley D D C, Cook S and Durrant J R 2005 Device annealing effect in organic solar cells with blends of regioregular poly(3-hexylthiophene) and soluble fullerene *Appl. Phys. Lett.* **86** 063502

[12] Yang F and Forrest S R 2008 Photocurrent generation in nanostructured organic solar cells *ACS Nano* **2** 1022–32

[13] Yang F, Shtein M and Forrest S R 2005 Controlled growth of a molecular bulk heterojunction photovoltaic cell *Nat. Mater.* **4** 37–41

[14] Kim M, Kim J, Cho J C, Shtein M, Guo L J and Kim J 2007 Flexible conjugated polymer photovoltaic cells with controlled heterojunctions fabricated using nanoimprint lithography *Appl. Phys. Lett.* **90** 123113

[15] Chou S Y, Krauss P R and Renstrom P J 1995 Imprint of sub-25 nm vias and trenches in polymers *Appl. Phys. Lett.* **67** 3114–6

[16] Chou S Y, Krauss P R and Renstrom P J 1996 Imprint lithography with 25-nanometer resolution *Science* **272** 85–7

[17] Barbero D R, Saifullah M M, Hoffmann P, Mathieu H J, Anderson D, Jones G A C, Welland M E and Steiner U 2007 High-resolution nanoimprinting with a robust and reusable polymer mold *Adv. Funct. Mater.* **17** 2419–25

[18] Tan H, Gilbertson A and Chou S Y 1998 Roller nanoimprint lithography *J. Vac. Sci. Technol.* B **16** 3926–8

[19] Ahn S H and Guo L J 2008 High-speed roll-to-roll nanoimprint lithography on flexible plastic substrates *Adv. Mater.* **20** 2044–9

[20] Heidari B, Maximov I, Sarwe E L and Montelius L 1999 Large scale nanolithography using nanoimprint lithography *J. Vac. Sci. Technol.* B **17** 2961–4

[21] Chou S Y, Krauss P R, Zhang W, Guo L and Zhuang L 1997 Sub-10 nm imprint lithography and applications *J. Vac. Sci. Technol.* B **15** 2897–904

[22] Austin M D, Ge H, Wu W, Li M, Yu Z, Wasserman D, Lyon S A and Chou S Y 2004 Fabrication of 5 nm linewidth and 14 nm pitch features by nanoimprint lithography *Appl. Phys. Lett.* **84** 5299–301

[23] Brown T M, Kim J S, Friend R H, Cacialli F, Daik R and Feast W J 1999 Built-in field electroabsorption spectroscopy of polymer light-emitting diodes incorporating a doped poly(3,4-ethylene dioxythiophene) hole injection layer *Appl. Phys. Lett.* **75** 1679–81

[24] Cheyns D, Poortmans J, Heremans P, Deibel C, Verlaak S, Rand B P and Genoe J 2008 Analytical model for the open-circuit voltage and its associated resistance in organic planar heterojunction solar cells *Phys. Rev.* B **77** 165332

[25] Jung G-Y, Li Z, Wu W, Chen Y, Olynick D L, Wang S-Y, Tong W M and Williams R S 2005 Vapor-phase self-assembled monolayer for improved mold release in nanoimprint lithography *Langmuir* **21** 1158–61

[26] Schift H, Saxer S, Park S, Padeste C, Pieles U and Gobrecht J 2005 Controlled co-evaporation of silanes for nanoimprint stamps *Nanotechnology* **16** S171–5

[27] Rolin C, Steudel S, Myny K, Cheyns D, Verlaak S, Genoe J and Heremans P 2006 Pentacene devices and logic gates fabricated by organic vapor phase deposition *Appl. Phys. Lett.* **89** 203502

[28] Rolin C, Vasseur K, Schols S, Jouk M, Duhoux G, Müller R, Genoe J and Heremans P 2008 High mobility electron-conducting thin-film transistors by organic vapor phase deposition *Appl. Phys. Lett.* **93** 033305

[29] Vanlaeke P *et al* 2006 P3HT/PCBM bulk heterojunction solar cells: relation between morphology and electro-optical characteristics *Sol. Energy Mater. Sol. Cells* **90** 2150–8

[30] Zhao Y, Yuan G, Roche P and Leclerc M 1995 A calorimetric study of the phase transitions in poly(3-hexylthiophene) *Polymer* **36** 2211–4

[31] Hugger S, Thomann R, Heinzel T and Thurn-Albrecht T 2004 Semicrystalline morphology in thin films of poly(3-hexylthiophene) *Colloid Polym. Sci.* **282** 932–8

[32] Kim Y, Choulis S A, Nelson J, Bradley D C, Cook S and Durrant J R 2005 Device annealing effect in organic solar cells with blends of regioregular poly(3-hexylthiophene) and soluble fullerene *Appl. Phys. Lett.* **86** 063502

[33] Campoy-Quiles M, Etchegoin P G and Bradley D D C 2005 Exploring the potential of ellipsometry for the characterisation of electronic, optical, morphologic and thermodynamic properties of polyfluorene thin films *Synth. Met.* **155** 279–82

[34] Dai H, Hafner J H, Rinzler A G, Colbert D T and Smalley R E 1996 Nanotubes as nanoprobes in scanning probe microscopy *Nature* **384** 147–50

[35] Martinez J, Yuzvinsky T D, Fennimore A M, Zettl A, García R and Bustamante C 2005 Length control and sharpening of atomic force microscope carbon nanotube tips assisted by an electron beam *Nanotechnology* **16** 2493–6

[36] Beek W J E, Wienk M M and Janssen R A J 2004 Efficient hybrid solar cells from zinc oxide nanoparticles and a conjugated polymer *Adv. Mater.* **16** 1009–13

[37] Beek W J E, Wienk M M and Janssen R A J 2006 Hybrid solar cells from regioregular polythiophene and ZnO nanoparticles *Adv. Funct. Mater.* **16** 1112–6

[38] Gilot J, Barbu I, Wienk M M and Janssen R A J 2007 The use of ZnO as optical spacer in polymer solar cells: theoretical and experimental study *Appl. Phys. Lett.* **91** 113520

[39] Gilot J, Wienk M M and Janssen R A J 2007 Double and triple junction polymer solar cells processed from solution *Appl. Phys. Lett.* **90** 143512

[40] Duché D, Escoubas L, Simon J-J, Torchio P, Vervisch W and Flory F 2008 Slow bloch modes for enhancing the absorption of light in thin films for photovoltaic cells *Appl. Phys. Lett.* **92** 193310